

April 1986

T.H. Nicol, R.C. Niemann and J.D. Gonczy

Fermi National Accelerator Laboratory, P. O. Box 500, Batavia, IL, 60510, USA

The design of a suspension system for the Superconducting Super Collider (SSC) presents many interesting problems to the cryostat designer. The suspension system must be strong enough to maintain the position of the cold mass during shipping, installation, and potential seismic conditions, it must be structurally stable over the anticipated 20 year life of the machine, and it must meet these constraints within the confines of a very strict allowable heat load. This paper describes various design alternatives considered for the SSC suspension and details the design and analysis of the reentrant post type supports chosen for the project. The results of structural, creep, and thermal tests on prototype assemblies are compared with predicted results.

INTRODUCTION

Suspension systems in superconducting magnets play many roles over the course of a magnet's life. They must maintain the position of the cold mass during shipping, installation, repeated cooldowns, and seismic excitation, they must be positionally stable over the expected operational period, and they must represent a high thermal impedance to heat conducted from the outside world. The magnets proposed for the Superconducting Super Collider (SSC) are very large¹, which means that their suspension system structural loads are also large. The allowable load on the refrigeration system is small, meaning that their thermal path lengths must be long and that the support materials must have low thermal conductivities. Table 1 summarizes the relevant geometric parameters, anticipated structural loads, and allowable heat loads for SSC magnets.

DESIGN ALTERNATIVES

During the evolution of the SSC cryostat design, several candidate suspension systems were considered. Each is described briefly below and illustrated in Fig. 1.

(a) Tension Straps

One of the first suspension alternatives consisted of a series of straps fabricated by winding epoxy impregnated fiber reinforced plastic (FRP) tape around an oval mandrel. The cold mass is hung from these straps using spherical bearings. One end is attached to the vacuum vessel, the other is attached to the cold mass. The bearings allow the cold mass to shrink axially and radially during cooldown, preventing shear and bending loads in the straps. Fig. 1(a) illustrates a typical tension strap suspension point.

The drawbacks to this concept are two-fold. First; given five support points, each with two vertical and one horizontal restraint, plus an axial cold mass anchor consisting of two angled straps, the tension strap suspension requires seventeen penetrations through heat shields and multi-layer insulation (MLI). Second; adjustment of the cold mass position during assembly is complicated by the number of adjustment points and gives no assurance that all supports are loaded uniformly.

(b) Compression Struts

A variation on the tension strap concept consists of struts loaded in compression as shown in Fig. 1(b). Rather than using FRP tape, compression struts use FRP material pultruded into solid rods. They might equally well be fabricated from composite tubes depending on the results of a buckling analysis. This design suffers the same drawbacks noted for tension straps.

(c) Elliptical Arch

A third, rather unique support concept consists of an elliptical arch acting as a beam structure to support the cold mass. The arch is fabricated from a titanium foil and composite laminate. The titanium acting as the principal load carrying material, and the composite acting to prevent local buckling of the foil. Such a design is relatively insensitive to load direction and is thus attractive in a design subjected to random loads. Unfortunately, this design uses more radial space than other configurations and imposes a significant load on the refrigeration system. A typical arch support is depicted in Fig. 1(c).

(d) Support Post

As a means of minimizing the number of shield and MLI penetrations and the number of adjustment points, early SSC suspension system designs employed a post-type structure consisting of a thin-wall composite tube attached to metal flanges at the vacuum vessel, cold mass, and thermal intercept locations. A five support system effected using post supports requires only seven penetrations through the thermal shields and MLI (including the anchor) compared with seventeen penetrations required when using tension straps or compression struts. Posts also require little radial space and are very easy to heat intercept and adjust. Fig. 1(d) illustrates a post support employed on the thermal and magnetic models of an early SSC magnet design.

SUPPORT POST DESIGN DEVELOPMENT AND ANALYSIS

The support post used on the first model magnet assemblies was far from being optimal. The primary objection was the length which necessitated an extension to the vacuum vessel at each support point. The length was required to maintain low heat loads. In addition, this length gave rise to large post deflections caused by off-centering magnetic forces. Shortly after the initial testing of prototype assemblies, a cold iron magnet design was chosen for subsequent models, eliminating the concerns about magnetic forces and enabling the coil to be positioned off-center with respect to the vacuum vessel. Using the original straight post as a starting reference, a modified post has been developed by 'folding' the assembly into itself, thereby maintaining the length required for thermal considerations and lowering the profile such that it fits within the confines of the vacuum vessel. Fig. 2 illustrates a cross-section of the post itself. Fig. 3 shows how it is incorporated into the SSC magnet cryostat.

One of the major issues in this design is the attachment of the composite tubes to the metal flanges. Epoxy joints are common practice, but their long term reliability is difficult to guarantee, particularly under repeated expansion/contraction cycles. All of the joints in the SSC post supports are assembled by shrink fitting the outer flanges onto the tube/backing ring combination. The radial contact pressure generated at each joint resists slipping of the joints under tensile or compressive loads and overturning due to applied moments. Using the notation in Fig. 4 for reference, the forces required to cause a joint to slip are given by:^{2,3}

$$F_1 = P_1(2\pi b t \mu_1) \quad ; \quad F_2 = P_2(2\pi c t \mu_2)$$

where

$$P_1 = \frac{P_2(K_4 + K_5) - \Delta_2}{K_6} \quad ; \quad P_2 = \frac{\Delta_1 K_6 + \Delta_2(K_1 + K_2)}{(K_4 + K_5)(K_1 + K_2) - K_3 K_6}$$

$$K_1 = \frac{b}{E_1} \frac{b^2 + a^2}{b^2 - a^2} - \nu_1 ; K_2 = \frac{b}{E_2} \frac{c^2 + b^2}{c^2 - b^2} + \nu_2 ; K_3 = \frac{b}{E_2} \frac{2c^2}{c^2 - b^2}$$

$$K_4 = \frac{c}{E_2} \frac{d^2 + c^2}{d^2 - c^2} + \nu_2 ; K_5 = \frac{c}{E_2} \frac{c^2 + b^2}{c^2 - b^2} - \nu_2 ; K_6 = \frac{c}{E_2} \frac{2b^2}{c^2 - b^2}$$

The bending moments required to overturn the joint are given by:

$$M_1 = 4P_1 \mu_1 b^2 t \quad ; \quad M_2 = 4P_2 \mu_2 c^2 t$$

Given a maximum applied axial force or bending moment at any joint one can calculate the required contact pressure and thus the design interference. A typical set of joint parameters is shown in Table 2.

A finite element analysis was performed on the body of the post assembly to check the stresses in the composite tubes and to determine whether stress concentrations developed as a result of the abrupt change in section at each joint. The mesh for the finite element model is shown in Fig. 5. The arch structure at the top of the model serves as the load application point and simulates a load applied at the coil centerline. The results from this analysis indicate no unusual stress concentrations anywhere in the assembly. Fig. 6 includes the deflections and stresses of prototype post assemblies predicted using this model.

TESTING

(a) Structural Testing

The finite element analysis described above pointed out relatively high bending stresses at the base of the inner and outer composite tubes due to lateral loads applied at the cold mass centerline. A bending test program was undertaken to verify this analysis and to determine actual failure modes. Displacements were measured at the coil centerline location and at each thermal intercept. Strain gages were mounted on the inner and outer tubes at positions where the finite element analysis predicted the two tubes to be equally stressed. Fig. 6 illustrates the results from these measurements.

In addition to the bending tests, each assembly was tested in tension and compression to verify the integrity of the shrink fit joints. The load carrying capacity of the posts in this mode exceeds the capacity of the test machine (10000 kg) which is 40 percent greater than the maximum design load corresponding to 5 g's.

The physical testing turned up an unanticipated design problem. Although the predicted and measured bending stresses were below the ultimate strength of the tube material, the inner tube exhibited a tendency to buckle locally at its base, causing premature failure of the post assembly. The solution to this problem has since been addressed and is discussed in the concluding remarks below.

(b) Thermal Testing

Thermal measurements were performed to verify predicted estimates of heat conduction through the post assembly. Estimated loads to 80K, 20K, and 4.5K were 1136.0, 103.5, and 19.1 mW respectively. Measured heat loads at these same points were 990.0, 102.0, and 26.6 mW for a single post. The slight differences between the measured and predicted values are easily attributable to variations in published and actual thermal conductivities for G-10, small contributions from radiative heat transfer which are not included in the predictions, and contributions from the measurement instrumentation itself.^{5,6}

(c) Creep Testing

There is little reason to be concerned about creep in the composite post tubes

occur in the shrink fit joints. As a result of this concern, three typical joints were instrumented, assembled, and monitored to observe the stress relaxation in the composite tubes and clamp rings at a temperature of 40.5 C. This temperature is consistent with the SSC pre-installation storage environment. The results from these tests, when extrapolated to the 20 year life of the SSC, indicate a stress relaxation of 3 percent. This stress reduction manifests itself in reduced contact pressure at the shrink fit interface with subsequent loss in axial and overturning moment restraint. Considering that the highest stresses occur in the 80K joint and that each joint is designed to restrain two times its expected load, creep effects do not appear to be a detriment to the post concept.

CONCLUSIONS

Due to the failure mode uncovered during the structural testing of the first support posts, some design changes have been implemented. The diameters of both the inner and outer tubes have been increased from 10.16 cm and 12.70 cm respectively to 12.7 and 17.78 cm. The increased diameters yield a higher bending stiffness and reduce the tendency toward local buckling of the composite material without significantly increasing the overall heat load.

Investigations into carbon fiber composites are in process. Such materials could conceivably increase the stiffness of the assembly further and, at the same time, decrease the heat load to 4.5K. The added stiffness afforded by these materials helps both the local buckling problem and the response of the system to the harmonic loads encountered during seismic upsets.

The support post concept remains a sound design choice for the SSC. Ongoing and future work serves only to enhance its overall performance.

ACKNOWLEDGEMENTS

The authors would like to thank Messrs. R. Zink, C. Miller, and R. Dixon for their design development efforts and Messrs. J. Otavka, W. Boroski, M. Frett, D. Validis, and J. Tweed for their help during prototype testing.

The work as presented was performed at Fermi National Accelerator Laboratory which is operated by Universities Research Association, Inc. under contract with the U.S. Department of Energy.

REFERENCES

- 1 Fisk, H.E., et al, 'The Ironless Cos θ Magnet Option for the SSC', IEEE Transactions on Nuclear Science, vol. NS-32 (1985), pp.3456-3465.
- 2 Roark, R.J. and Young, W.C., Formulas for Stress and Strain, 5th edition, McGraw-Hill, New York (1975), pp.424-428, 503-506.
- 3 Juvinall, R.C., Stress Strain and Strength, McGraw-Hill, New York (1967), pp.112-141.
- 4 'ANSYS Engineering Analysis System User's Manual', Swanson Analysis Systems, Inc., Houston, PA (1983).
- 5 Reed, R.P., and Clark, A.F., Materials at low temperatures, American Society For Metals, Metals Park, Ohio (1983), pp.95-96.
- 6 Bensinger, J.R., 'Properties of Cryogenic Grade Laminates', IEEE Conference (1979), Boston, MA.

Assembly length: 16.6 m

Assembly weights:

Cold mass assembly	7160 kg
20K shield assembly	225 kg
80K shield assembly	300 kg
Total	7685 kg

(1537 kg/support for 5 supports)

Structural dynamic environments:

Transportation*
 5g vertical
 3g axial
 2g lateral

Handling*
 5g vertical
 3g axial
 2g lateral

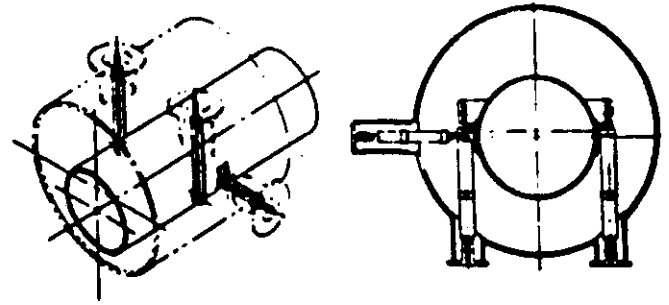
Seismic
 0.3g earthquake

Maximum allowable bending stresses: 0.5 x mat'l ultimate

Allowable heat loads per magnet:•
 6.7 watts to 80K
 0.7 watts to 20K
 0.2 watts to 4.5K

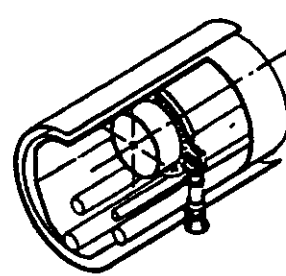
- * Removable shipping restraints allowed
- Includes supports, anchor, and contingency

Table 1 SSC magnet geometry and loads

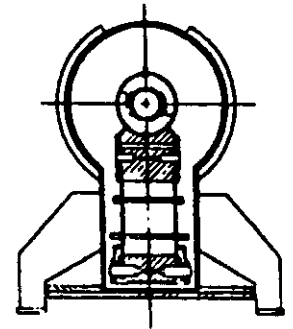


(a) Tension Straps

(b) Compression Struts



(c) Elliptical Arch



(d) Straight Post

Fig. 1 SSC suspension options

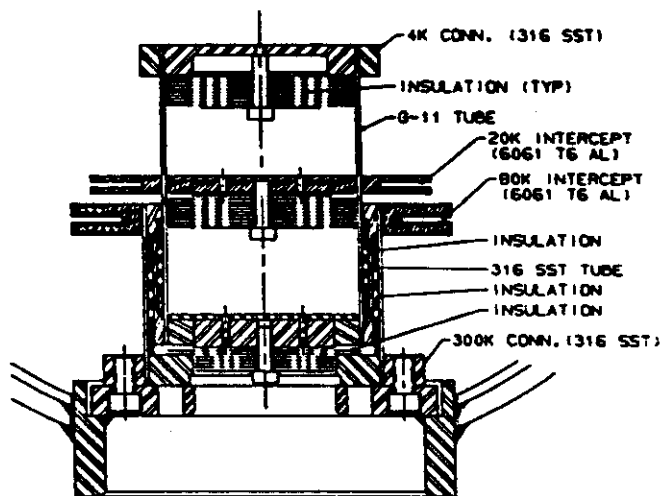


Fig. 2 Folded post cross section

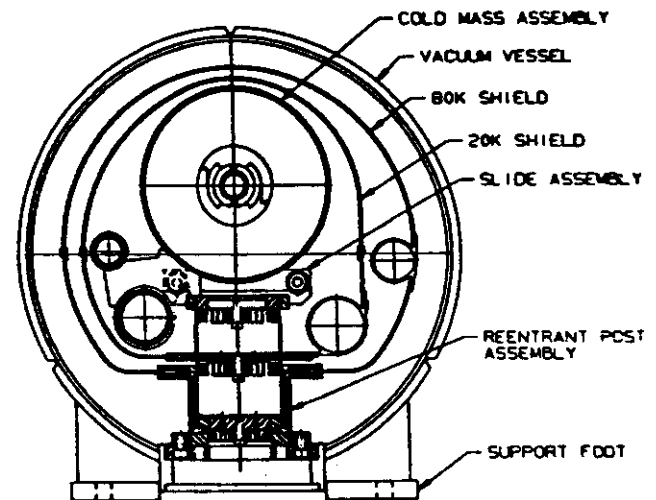
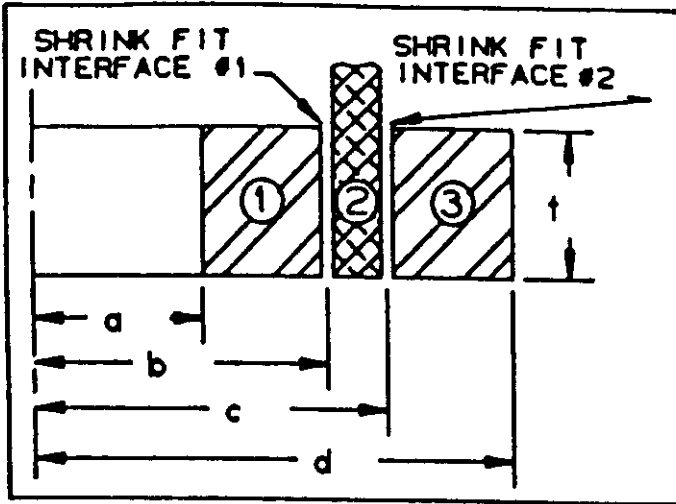


Fig. 3 SSC magnet cryostat cross section



MATERIAL PROPERTIES

Elastic Modulus: E_1, E_2, E_3
 Poisson's Ratio: ν_1, ν_2, ν_3

INTERFACE PROPERTIES

Contact Pressure: P_1, P_2
 Radial Interference: Δ_1, Δ_2
 Coefficient of Friction: μ_1, μ_2

Joint ¹	Diametral Interference (cm)	Contract Pressure (MPa)	Force to Slip ² (kg)	Resisting Moment ² (kg-m)
300K	0.033	63	18880	1060
80K	0.064	47	14075	795
Intermed	0.046	119	25340	1010
20K	0.025	27	3630	105
4.5K	0.028	51	10820	435

¹ 12.70 x 17.78 cm post

² Assumed coefficient of friction = 0.3

Fig. 4 Shrink fit joint nomenclature

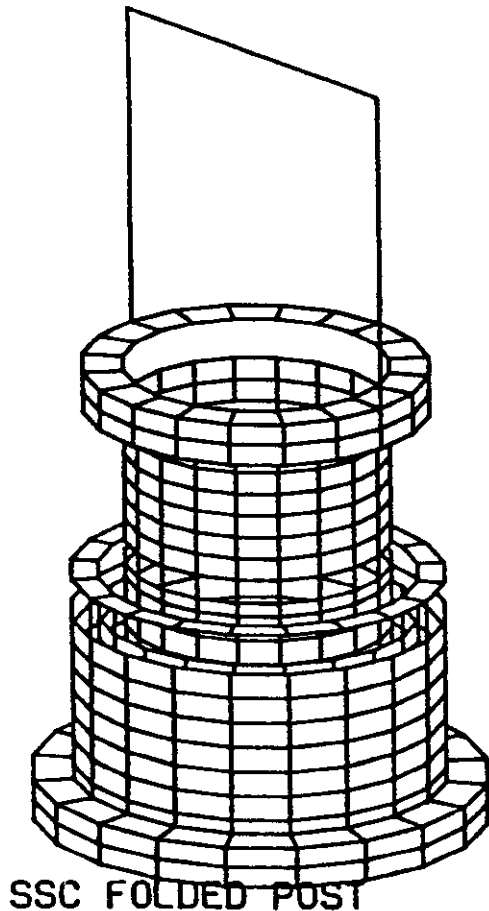


Table 2 Shrink fit joint performance data

